Performance Comparisons of Maneuvering Vehicles Returning from Orbit

Michael E. Tauber* and Lily Yang†
NASA Ames Research Center, Moffett Field, California

A comparison of skipping and gliding flight paths is presented, followed by a discussion of gliding high-speed turning maneuvers and lateral flight ranges. Whereas skipping vehicles can attain longer ranges than gliding vehicles, the deceleration loads can be an order of magnitude higher, even for shallow entries. To withstand the increased structural loads, major components such as the fuselage and wings must be two and three times heavier, respectively. Also, the heating rates during skipping flight are four to five times higher, for an entry angle of only 5.7 deg, thus requiring a much heavier thermal protection system than for gliding flight. For a gliding aerodynamic maneuver consisting of a 90-deg turn initiated at entry, a vehicle with a maximum lift-to-drag (L/D) ratio of 2.9 is able to glide another 2750 km after completing the turn to achieve a total lateral range of 8000 km. The same vehicle can make a 180-deg high-speed turn during which a lateral distance of 5000 km would be covered; however, the additional range after completing the turn is only 750 km. The present lateral range calculations also showed that a choice of global landing sites can be achieved with $L/D = 3.23$, or a 5% lower L/D value than obtained from previous formulations. The aerodynamic heating of the vehicle is strongly affected by maneuvering. The peak heating intensity increases by about 30 and 40% during 90 and 180-deg turns, respectively, compared to unbanked flight; however, the total heat input is less since the duration of the heating pulse is reduced.

Nomenclature

A = reference area of entry vehicle
a = acceleration
C = constant, Eq. (20)
C_D = drag coefficient
C_L = lift coefficient
D = drag
g = acceleration of gravity
L = lift
l = lateral distance
M = see Eq. (20)
m = vehicle mass
N = see Eq. (20)
n = structural load factor
$\dot{q}$ = heat-transfer rate into the body per unit area
R_0 = planetary radius
r_n = body nose radius
S = distance along Earth surface (range)
s = distance along trajectory
T_w = equilibrium wall temperature
t = time
V = flight velocity
V_f = final velocity at end of turn
V_i = initial velocity at beginning of turn
V_s = surface grazing (circular) satellite speed (7.9 km/s)
W = vehicle weight
x = distance measured along body surface
Y = side force
α = angle of attack
β = inverse atmospheric-density scale height
γ = flight-path angle
Δ = wing leading-edge sweep angle
ε = surface emissivity
ρ = freestream density
ρ_0 = sea-level atmospheric density
σ = Stefan-Boltzmann constant
ϕ = bank or roll angle, measured from the horizontal
ψ = turn angle

Subscripts

E = entry condition
FP = flat plate
f = final value
GL = glide
i = initial value
LE = wing leading edge
max = maximum
n = normal
SK = skip
t = tangential
w = wall
0 = stagnation point
$()_*$ = flight conditions for peak deceleration or peak heating rate

Introduction

USING high-lift vehicles when returning from low-Earth orbit has many advantages. A primary benefit of lift is the ability to achieve a large longitudinal range. Lift also provides the capability to maneuver within the atmosphere. Maneuverability enhances mission flexibility and increases the choice of landing sites. Lift also can be used to alleviate the deceleration loads and aerodynamic heating accompanying atmospheric entries. The resultant moderation of the entry environment benefits the occupants of the vehicle and permits lower structural and thermal protection weights. The present paper begins with a comparison of skipping and gliding flight paths. Trajectory characteristics that will be compared are longitudinal range, deceleration and structural load factors, and aerodynamic heating at two key vehicle locations. The presentation proceeds with a discussion of gliding high-speed turning maneuvers and lateral flight ranges. The aerodynamic heating pulses during longitudinal flight and lateral maneuvers are compared as well.

Presented as Paper 87-2490 at the AIAA Atmospheric Flight Mechanics Conference, Monterey, CA, Aug. 17–19, 1987; received Sept. 9, 1987; revision received Dec. 30, 1987.

*Research Scientist. Associated Fellow AIAA.
†Professional Staff Member, Sterling Software, Palo Alto, CA.

Analysis

The analysis begins with the formulation of the characteristic features of skipping and gliding trajectories. Next, convective heating relations and the application to the stagnation point of a hypothetical vehicle and a representative point on the wing leading edge are discussed. The analysis concludes with the derivation of relations for lateral turns and the distances that are covered during the maneuvers.

Throughout the analysis, efforts are made to obtain relatively simple analytic solutions that retain the basic physical phenomena and have been verified. Although numerical solutions potentially can be more precise, valuable physical insight is obscured frequently. Approximations that are consistent with the overall accuracy of the analysis are used to make comparisons valid.

Trajectories

The formulation of the trajectory relations is based on Ref. 1. The equations of motion normal and tangential to the flight path are for unpowered flight in a nonrotating atmosphere

$$L = W\cos\gamma - mV^2\left(\frac{\cos\gamma}{R_0} + \frac{d\gamma}{ds}\right) \tag{1a}$$

and

$$D = W\sin\gamma - m\frac{dV}{dt} \tag{1b}$$

For manned vehicles, the flight-path angles must be shallow to limit the deceleration forces, as will be shown later. When the flight-path angles are small, Eqs. (1) simplify to

$$L = W - mV^2\left(\frac{1}{R_0} + \frac{d\gamma}{ds}\right) \tag{2a}$$

and

$$D = -m\frac{dV}{dt} \tag{2b}$$

The deceleration force experienced by the vehicle crew can be written as

$$a/g = [(a_t/g)^2 + (a_n/g)^2]^{\frac{1}{2}} \tag{3a}$$

where, from Eq. (2b),

$$a_t = -D/m \tag{3b}$$

and

$$a_n = L/m \tag{3c}$$

Therefore

$$\frac{a}{g} = -\frac{dV}{dt}\left(\frac{1}{g}\right)\left[1 + \left(\frac{L}{D}\right)^2\right]^{\frac{1}{2}} \tag{3d}$$

where L/D is the lift-to-drag ratio. From the above trajectory expressions, equations applicable to skipping and gliding flight paths will be derived.

Skipping Flight Paths

A skipping trajectory generally results when a vehicle with large positive (upward) lift enters the atmosphere at hypervelocity speeds. As the vehicle descends into the atmosphere, the lift force grows rapidly as the dynamic pressure increases. The rapid growth of the lift force causes the vehicle to make a longitudinal turn that carries it to a higher altitude or entirely out of the atmosphere. After leaving the sensible atmosphere, the path becomes a portion of a Keplerian ellipse with one focus at the center of the Earth. At the conclusion of each exoatmospheric ballistic trajectory, the vehicle re-enters the atmosphere with the same velocity it had upon ejection. The magnitude of the flight-path angle is also the same on entry as it was at exit, but the direction is reversed.

During the longitudinal turn, the aerodynamic lift must be much larger than the weight in Eq. (1a); in addition,

$$\frac{\cos\gamma}{R_0} \ll \frac{d\gamma}{ds}$$

Therefore, Eq. (1a) can be written as

$$L = \frac{1}{2}\rho V^2 C_L A = -mV^2\frac{d\gamma}{ds} \tag{4}$$

Assuming an exponential atmospheric density variation with altitude, where ρ_0 is the sea-level density and β the inverse of the scale height,

$$\rho = \rho_0 e^{-\beta y} \tag{5}$$

and combining Eq. (5) with the geometric relation

$$\frac{dy}{ds} = -\sin\gamma$$

yields

$$\frac{d\rho}{ds} = -\beta\rho\sin\gamma \tag{6}$$

Substituting Eq. (6) into Eq. (4) gives

$$(C_L A/2m\beta)\,d\rho = -\sin\gamma\,d\gamma \tag{7a}$$

which can be readily integrated to yield

$$(C_L A/2m\beta)(\rho - \rho_E) = \cos\gamma - \cos\gamma_E \tag{7b}$$

In general, the air density at entry can be neglected in Eq. (7b). For entry angles of less than approximately 30 deg, which include all cases of interest here, Eq. (7b) can be simplified somewhat further by expanding the cosine in series and, if only first-order terms in γ are retained,

$$(C_L A/m\beta)\rho = \gamma_E^2 - \gamma^2 \tag{7c}$$

To relate the velocity and flight-path angle, Eq. (4) is written in the form

$$L = -mV\frac{d\gamma}{dt} \tag{8a}$$

and if Eq. (2b) is used to eliminate the time term, then

$$d\gamma = \frac{L}{D}\frac{dV}{V} \tag{8b}$$

Upon integration

$$V = V_E \exp[(\gamma - \gamma_E)/(L/D)] \tag{8c}$$

and Eqs. (7c) and (8c) define the atmospheric portion of the trajectory.

To find the altitude at which maximum deceleration occurs, Eqs. (7c) and (8c) are combined to eliminate γ. The resultant equation is then solved for the product ρV^2 and the maximum value of ρV^2 gives the altitude for peak deceleration, which is

$$\rho_* = \frac{m\beta}{2C_D A}\frac{L}{D}\left\{\left[1 + \frac{4\gamma_E^2}{(L/D)^2}\right]^{\frac{1}{2}} - 1\right\} \tag{9a}$$

For small entry angles,

$$\frac{4\gamma_E^2}{(L/D)^2} \ll 1$$

and using the binomial series to expand the square-root term gives

$$\rho_* = [(m\beta\gamma_E^2)/(C_D A)](1/L/D) \tag{9b}$$

which is the altitude at the bottom of the skip, where $\gamma = 0$, and

$$V_* = V_E \exp[-\gamma_E/(L/D)] \tag{10}$$

Now Eqs. (9b), (10), and (2b) are combined to find the peak value of the tangential deceleration, which is substituted into Eq. (3d) to yield the total deceleration

$$\left(\frac{a}{g}\right)_{\max} = \frac{\beta\gamma_E^2 V_E^2 \exp[-2\gamma_E/(L/D)]}{2g}\left[1+\frac{1}{(L/D)^2}\right]^{\frac{1}{2}} \tag{11}$$

The structural loads are proportional to the normal acceleration, which also peaks at the bottom of the skip where the radius of curvature of the flight path has its minimum value. Using Eq. (3c) and substituting Eqs. (9b) and (10) into the expression for the lift gives

$$(a_n)_{\max} = \{\beta\gamma_E^2 V_E^2 \exp[-2\gamma_E/(L/D)]\}/2 \tag{12}$$

The maximum range of the skip vehicle is determined by summing the distances covered during the ballistic phases and adding the distances flown during each atmospheric dip. The range for the sum of the ballistic coast trajectories is derived in Ref. 1 and is

$$S_1 = 2R_0 \sum_{n=1}^{\infty} \tan^{-1}\left[\frac{\sin\gamma_E \cos\gamma_E}{\left(\frac{V_s}{V_E}\right)^2 \exp[4(n-1)\gamma_E/(L/D)] - \cos^2\gamma_E}\right] \tag{13}$$

The intra-atmospheric contribution to the range is calculated by making the flat-Earth assumption. Using Eq. (2b) and $dS_2 = V\cos\gamma\, dt$ yields the incremental range

$$dS_2 = -\frac{2m}{C_D A}\frac{\cos\gamma}{\rho V}\, dV \tag{14a}$$

Substituting for density and velocity from Eqs. (7b) and (8b) and writing the integral gives

$$S_2 = -\frac{1}{\beta}\int_{\gamma_E}^{0} \frac{\cos\gamma\, d\gamma}{\cos\gamma - \cos\gamma_E + (C_D A/2m\beta)(L/D)\rho_i} \tag{14b}$$

which can be integrated to yield the approximate expression

$$S_2 \approx \frac{\cot\gamma_E}{\beta}\ell n\left(\frac{4m\beta\sin^2\gamma_E}{C_D A(L/D)\rho_i}\right) + \frac{\gamma_E}{\beta} \tag{14c}$$

where ρ_i represents the altitude at which the intra- and exo-atmospheric trajectories are matched. In deriving Eq. (14c), it has been assumed that the altitude at which the trajectories are matched must be sufficiently high so that

$$\frac{C_D A}{2m\beta}\frac{L}{D}\rho_i \ll \cos\gamma_E$$

If the preceding inequality is not satisfied, the amplitude of the oscillations has become small and the vehicle no longer leaves the atmosphere. In this case, Eq. (4) is not applicable and the last phase of the flight path becomes an equilibrium glide, which will be discussed next.

Equilibrium Glide Flight Paths

When a high-lift vehicle enters the atmosphere from a low-Earth orbit at an angle of less than about 1 deg, significant altitude oscillations can be avoided and a smooth glide results. In that case, Eq. (2a) can be written as

$$L = W - (mV^2/R_0) \tag{15a}$$

since

$$\frac{d\gamma}{ds} \ll \frac{1}{R_0}$$

The preceding expression, Eq. (15a), describes the equilibrium glide trajectory, such as that flown by the Space Shuttle, where the lift and centrifugal force balance the weight. The altitude-velocity relation comes directly from Eq. (15a) without requiring the exponential atmospheric density assumption, and is

$$\rho = \frac{2}{R_0}\left(\frac{m}{C_D A}\right)\left(\frac{1}{L/D}\right)\left(\frac{V_s^2}{V^2} - 1\right) \tag{15b}$$

Because the flight-path angle is very small, Eq. (2b) gives a good approximation. The deceleration is found by substituting Eqs. (2b) and (15b) into Eq. (3d), and is

$$-\frac{a}{g} = \left(1 - \frac{V^2}{V_s^2}\right)\left[1 + \frac{1}{(L/D)^2}\right]^{1/2} \tag{16a}$$

For a constant L/D, the maximum deceleration occurs as the flight velocity becomes small and approaches

$$-\left(\frac{a}{g}\right)_{\max} = \left[1 + \frac{1}{(L/D)^2}\right]^{1/2} \tag{16b}$$

The normal acceleration during an equilibrium glide is found by using Eqs. (3b) and (15a) to be

$$a_n = g[1 - (V^2/V_s^2)] \tag{17a}$$

which has a peak value of

$$a_n = g \tag{17b}$$

Therefore, the deceleration forces during gliding entry are benign, which is one reason why the Space Shuttle flies such a trajectory. For example, if $L/D = 1$, the maximum deceleration is about $1.4g$. [Peak decelerations during Shuttle entries are about 1.5–1.6g and occur near a speed of 1.5 km/s.[2] Although a glide trajectory is flown, the bank angle is modulated over a large range (± 60 deg) to reduce entry time and total heat input.]

To determine the range during the equilibrium glide, Eq. (2a) is written as

$$\rho = -\frac{2m}{C_D A}\frac{dV}{V\, ds} \tag{18}$$

Upon substituting Eq. (18) into Eq. (15b), the expression can be integrated directly to yield

$$S = s = \frac{1}{2}\left(\frac{L}{D}\right) R_0 \ell n\left(\frac{V_s^2 - V^2}{V_s^2 - V_E^2}\right) \tag{19}$$

Note that V_E must be less than V_s to ensure that the vehicle does not skip out of the atmosphere.

Aerodynamic Heating Rates

It is assumed that the heating rate per unit area can be written in the form

$$\dot{q} = C\rho^N V^M \tag{20}$$

where N and M can be assumed to be constant. Equation (20) applies in the flight regime for which boundary-layer theory is valid. Equation (20) is a good approximation for both laminar[3,4] and turbulent[5] convection at a catalytic surface in the absence of boundary-layer mass addition. The numerical values used in Eq. (20), taken from Refs. 3 and 5, are for the stagnation point and turbulent flat-plate heating, respectively. The laminar flat-plate heating expression comes from transforming the cone relation derived in Ref. 4. None of the constants in Eq. (20) were modified using flight data. (Values of N and M, and expressions for C are given in Ref. 6.) The assumption that the wall is fully catalytic is conservative and also makes Eq. (20) independent of the choice of heat-shielding material. Since C is a weak function of wall temperature, which is given by

$$T_w = (\dot{q}/\varepsilon\sigma)^{\frac{1}{4}} \tag{21}$$

it is necessary to iterate between Eqs. (20) and (21) to find the heating rate assuming radiative equilibrium at the wall.

The form of Eq. (20) is suitable for calculating the stagnation point and the flat-plate heat transfer. The wing leading-edge heating rate was computed using the swept-cylinder theory[6] in the form

$$\dot{q}_{LE} = [\tfrac{1}{2}(\dot{q}_0)^2 \cos^2\Delta + (\dot{q}_{FP})^2 \sin^2\Delta]^{\frac{1}{2}}(\cos\alpha) \tag{22}$$

where Δ is the leading-edge sweep angle.

The beginning of boundary-layer transition from laminar to turbulent flow is predicted using a modified correlation of local-length Reynolds number and local Mach number.[7] The original correlation for cones[7] was modified and extended to nonaxisymmetric bodies by adding transition data from Shuttle flight STS-1.[8] The length of the transitional boundary-layer region is assumed to be the same as the preceding laminar-flow distance. A linear variation is assumed between the laminar values and the fully established turbulent heating rates. Comparisons of laminar, transitional, and turbulent heating rates with Shuttle flight data[9] agreed well with this assumption.

Aerodynamic Maneuvers

A major benefit enjoyed by high-lift vehicles is the ability to maneuver within the atmosphere. The most basic maneuver is a banked turn, which also determines the lateral range of the vehicle, which can be very important.

Turns

A turn, or change of heading, occurs when a side force Y acts on the vehicle. The side force acts normal to the lift and drag, and is given by

$$Y = mV^2 \frac{d\psi}{ds} \tag{23}$$

where ψ is the lateral angle through which the trajectory has been turned from its initial direction. The side force results from rotating the lift force by banking the vehicle through an angle ϕ, and is

$$Y = L \sin\phi$$

By combining Eq. (2b) with Eq. (23) and the kinematic relation $V = ds/dt$, the change in the lateral flight-path angle becomes

$$d\psi = -\frac{Y}{D}\frac{dV}{V} \tag{24a}$$

Integrating the preceding equation and substituting for the side force gives an expression that is valid for any constant L/D trajectory

$$\psi = \frac{L}{D}(\sin\phi)\,\ell n\left(\frac{V_i}{V}\right) \tag{24b}$$

where V_i is the velocity at the beginning of the turn.

A logical choice for studying hypervelocity turning maneuvers is the equilibrium glide trajectory. Solving Eq. (24b) for the velocity and substituting into Eq. (15b) for banking flight gives the altitude as a function of the heading angle.[10]

$$\rho = \rho_0 e^{-\beta y} = \frac{2m}{R_0 C_D A (L/D)\cos\phi} \times \left[\left(\frac{V_s}{V_i}\right)^2 \exp[2\psi/(L/D)\sin\phi] - 1\right] \tag{25}$$

Equation (25) can be used to study a variety of maneuvers. For example, assume that the vehicle is to make a turn with a minimum loss of altitude. The optimum constant bank angle for this case is found by differentiating Eq. (25) with respect to ϕ and setting the result equal to zero yielding

$$\left(1 - \frac{2\psi}{(L/D)\tan^2\phi \sin\phi}\right)\left(\frac{V_s}{V_i}\right)^2 \exp[2\psi/(L/D)\sin\phi] - 1 = 0 \tag{26}$$

Equation (26) can be readily solved numerically for any combination of turning angle, initial velocity, and L/D.

Turning flight maneuvers impose an additional deceleration force on the vehicle. However, Eq. (3d) is still valid. Combining Eqs. (2b) and (15b) for turning flight gives

$$-\frac{dV}{dt} = \frac{g}{(L/D)\cos\phi}\left[1 - \left(\frac{V}{V_s}\right)^2\right] \tag{27a}$$

Substituting Eq. (27a) into Eq. (3d) yields the total deceleration

$$\frac{a}{g} = \frac{1 - (V/V_s)^2}{\cos\phi}\left[1 + \frac{1}{(L/D)^2}\right]^{\frac{1}{2}} \tag{27b}$$

Note that Eqs. (16a) and (27b) have the same form, with the exception of the $\cos\phi$ in the latter. The dependence on the bank angle given in Eq. (27b) agrees with numerical solutions for values up to about 75 deg.[11]

For gliding entry, the velocity at which peak convective heating occurs is[12]

$$V_* = [(M - 2N)/M]^{\frac{1}{2}} V_s \tag{28}$$

If the turn is initiated before peak heating occurs, then the altitude at the peak heating rate[12] is

$$\rho_* = \frac{2N}{M - 2N} K = \left(\frac{2N}{M - 2N}\right)\left(\frac{2}{R_0}\frac{m}{C_D A}\frac{1}{(L/D)\cos\phi}\right) \tag{29}$$

The maximum heating rate per unit area[11] is given by

$$\dot{q}_{max} = C\left(\frac{4N}{R_0}\frac{m}{C_D A}\frac{1}{(L/D)\cos\phi}\right)^N \left(\frac{V_s}{\sqrt{M}}\right)^M (M - 2N)^{M/2 - N} \tag{30}$$

Lateral Range

The problem of determining the lateral range of a gliding entry vehicle was first solved in an approximate manner[13] for a low L/D. Shortly thereafter, the solution was extended to somewhat higher L/D's.[11] More than a decade later, the problem was formulated and solved to cover the entire spectrum of achievable lift/drag ratios.[14] The following discussion draws on all three sources, i.e., Refs. 11, 13, and 14.

The elemental change in lateral range is related to the change in longitudinal range by

$$dl = \sin\psi\, ds \tag{31}$$

The longitudinal range comes from the equilibrium glide ex-

pression for banked flight, which is

$$\frac{ds}{R_0} = \frac{L}{D}\cos\phi\left(\frac{V\,dV}{V^2 - V_s^2}\right) \tag{32}$$

Combining Eqs. (24b), (31), and (32) results in

$$\frac{l}{R_0} = \frac{L}{D}\cos\phi\int_{V_i}^{V_f}\sin\left(\frac{L}{D}\sin\phi\,\ell n\frac{V_i}{V}\right)\left(\frac{V\,dV}{V^2 - V_s^2}\right) \tag{33}$$

Here, the first term under the integral is $\sin\psi$. For the case of a turn initiated upon entry at satellite speed, Eq. (33) was solved in Ref. 13 by assuming that, for small L/D,

$$\sin\psi = \psi$$

and then integrating Eq. (33), from $V_i = V_s$ to $V_f = 0$, to give

$$\frac{l}{R_0} = \frac{\pi^2}{48}\left(\frac{L}{D}\right)^2\sin 2\phi \tag{34a}$$

Note that the lateral range is a maximum when $\phi = 45$ deg. (In Ref. 11, $\sin\psi$ was expanded in a power series and numerical results were tabulated.) The more general solution of Ref. 13 gives, to second order,

$$\frac{l}{R_0} = \frac{\pi^2}{48}\left(\frac{L}{D}\right)^2\sin 2\phi\left[1 - \frac{0.608(L/D)^2\cos^2\phi}{4 + (L/D)^2\cos^2\phi}\right] \tag{34b}$$

and an optimum bank angle of approximately

$$\phi = 45\left[1 + \frac{(L/D)^2}{3.60(L/D)^2 + 20.65}\right] \tag{34c}$$

For practical purposes, the deviation of the optimum bank angle from 45 deg has little effect, and using a value of $\phi = 45$ deg in the brackets in Eq. (34b) agrees well with numerical solutions for $L/D \leq 3$.

In the integrations leading to Eqs. (34), it is implicitly assumed that the entire lateral maneuver is performed at a constant bank angle. This assumption can lead to errors for large L/D vehicles, which retain high velocities at the conclusion of the 90 deg turn. The velocity after completing a turn, V_f, is found from Eq. (24b) to be

$$V_f = V_i\exp[-\psi/(L/D)\sin\phi] \tag{35}$$

To maximize the range after completing a turn, the vehicle should be rolled to zero bank angle. The residual range in the vehicle's current direction is given by[10]

$$\frac{\Delta s}{R_0} = -\frac{1}{2}\frac{L}{D}\ell n\left[1 - \left(\frac{V_f}{V_s}\right)^2\right] \tag{36}$$

The residual range can be a large fraction of the total lateral distance flown, as will be shown subsequently.

Study Parameters

The study was intentionally performed without defining specific missions or vehicle configurations. However, the trajectories will be limited to reasonably shallow entry angles, suitable for manned vehicles. The heating rates will be analyzed at two locations on the vehicle: the stagnation point and a point on the wing leading edge.

Trajectories

Only trajectories having entry angles of 10 deg or less will be considered to maintain g forces within human tolerance. With adequate vertical lift, such trajectories exhibit multiple atmospheric skips. Specifically, skipping flight paths with entry angles of 5.73 (0.1 rad), 8.6, and 10 deg will be considered. The deceleration, structural load factors, and heating rates all peak during the first atmospheric skip since the entry velocity is highest. Therefore, only the conditions during the first skip need to be evaluated here. Obviously, the entire trajectory must be considered when calculating the range.

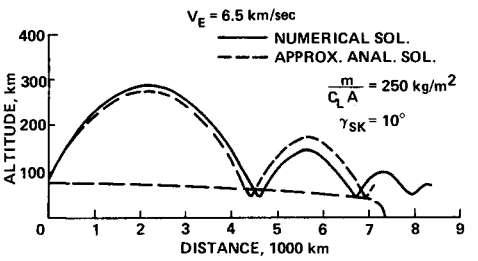

Fig. 1 Comparison of skipping and gliding entry trajectories.

Gliding flight results when the entry angle approaches zero, thereby eliminating this parameter. The aerodynamic parameters of ballistic coefficient and L/D can be combined for both skipping and gliding flight by using

$$\frac{m}{C_L A} = \frac{m}{C_D A}\frac{1}{L/D}$$

The angle of attack at maximum L/D is assumed to be 15 deg.

Heating Rates

The body dimensions and wing sweep required to evaluate the heating are chosen to be representative of a configuration having better aerodynamic performance than the Space Shuttle. (The Shuttle has a hypersonic maximum L/D approaching 2.) The two body locations at which heating is calculated are chosen because the stagnation point experiences only laminar flow, whereas the wing leading edge is also exposed to a transitional and turbulent boundary layer. The vehicle is assumed to have a fairly sharp nose with a radius of 10 cm. The wing leading edge is swept back at 75 deg. The leading-edge radius is 5 cm at a point 10 m from the wing/body juncture where the heating rate is calculated. The equilibrium wall temperatures are calculated assuming an emissivity value of 0.8.

Turns

Only turning maneuvers performed in gliding flight will be considered. Turns of 90 deg are studied since these determine the maximum lateral range. In addition, a more extreme case consisting of a 180 deg turn is also investigated. The maneuvering capabilities will be studied for maximum lift/drag ratios varying from 2 to 3.

Results

First, the aerodynamic and heating characteristics of skipping and gliding trajectories are compared. Next, maneuvering capabilities during gliding flight are presented. Last, the heating pulses for two maneuvering trajectories are compared with the heating rate experienced during longitudinal flight.

Trajectory Characteristics

The key trajectory characteristics of range, decelerations, loads, and heating are compared for shallow skipping and gliding entries.

In Fig. 1, skipping and gliding trajectories are shown for an entry velocity of 6.5 km/s. The skip vehicle enters the atmosphere at an angle of 10 deg; the entry angle for the gliding case is about 0.1 deg. The range during the first two skips was computed using Eqs. (13) and (14c). The exoatmospheric portion of the skips was calculated using Kepler's relations[15]; the exoatmospheric and endoatmospheric portions were matched at 90 km. Note the good comparison, especially for the first skip, with the exact numerical solution.‡ The maximum range for the skipping flight path is about 9500 km, or roughly 23%

‡The numerical solution was provided by John T. Wilson, Sterling Software, Palo Alto, CA.

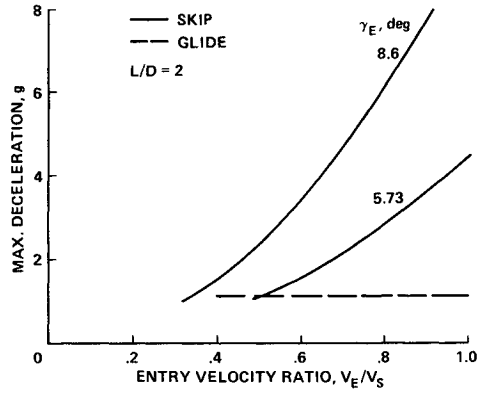

Fig. 2 Maximum total deceleration loads for skipping and gliding entries.

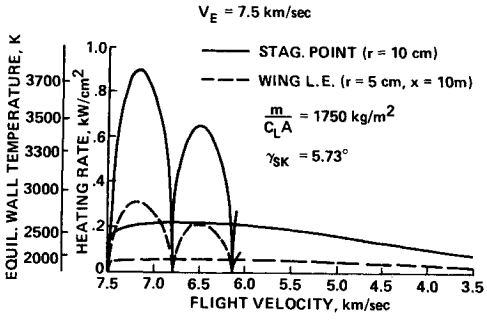

Fig. 3 Heating comparisons for skipping and gliding entries.

greater than the 7350 km of the glide. The peak total deceleration, which is experienced at the conclusion of the first skip, is 8.55g from Eq. (11), or within 5% of the 8.9-g value of the numerical solution.

The maximum total decelerations for two skipping trajectories having entry angles of 5.73 and 8.6 deg are compared with gliding entry in Fig. 2, using Eqs. (11) and (16b). When entering at circular-satellite speed, the vehicles flying the skipping trajectories experience four times and eight times the g loads of the glider for entry at 5.73 and 8.6 deg, respectively. The high deceleration loads encountered during skipping flight also result in much heavier vehicle structures as well as causing crew discomfort. The load factor ratios, calculated using Eqs. (12) and (17), translate into structural weight ratios[16] of 2 and 2.83 for delta wings, whereas fuselage weights are increased by factors of 1.52 and 1.87, respectively.

In Fig. 3, the aerodynamic heating is compared for a skipping entry at 5.73 deg and a gliding flight path at an entry velocity of 7.5 km/s. The stagnation-point heating rate is almost 900 W/cm^2, and the wing leading-edge value is over 300 W/cm^2 for the skipping case. The corresponding equilibrium wall temperatures are far beyond the radiative cooling capabilities of known materials. For the gliding entry, the stagnation-point heating rate reaches about 225 W/cm^2. However, the wing leading-edge peak heating rate is only about 60 W/cm^2, resulting in a wall temperature of 1900 K, which permits radiative cooling. Since gliding entry results in a more benign aerodynamic and heating environment, the following discussion of aerodynamic maneuvers will be confined to gliding flight paths.

Aerodynamic Maneuvers

The aerodynamic maneuvers studied consist of 90- and 180-deg hypervelocity turns and the range covered during and after the turns. In addition, the heating pulses during turning flight will be compared to heating encountered in longitudinal flight.

It is assumed here that a vehicle is to perform a high-speed turn with a minimum loss of altitude. Optimum bank angles are shown in Fig. 4 for turning angles of 90 and 180 deg as a function of L/D. The velocities at which the turns are begun vary from $0.8V_s$ to V_s; however, note the weak dependence of bank angle on initial velocity.

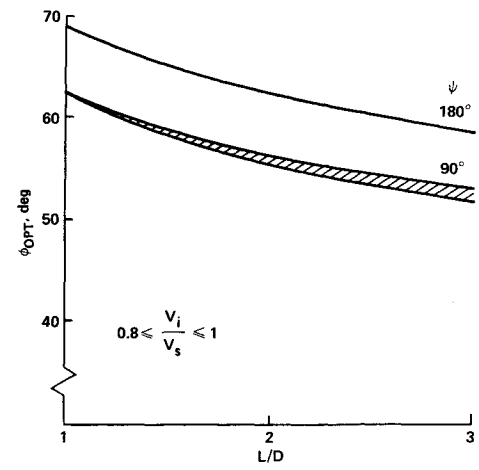

Fig. 4 Variation of optimum bank angle with lift/drag ratio.

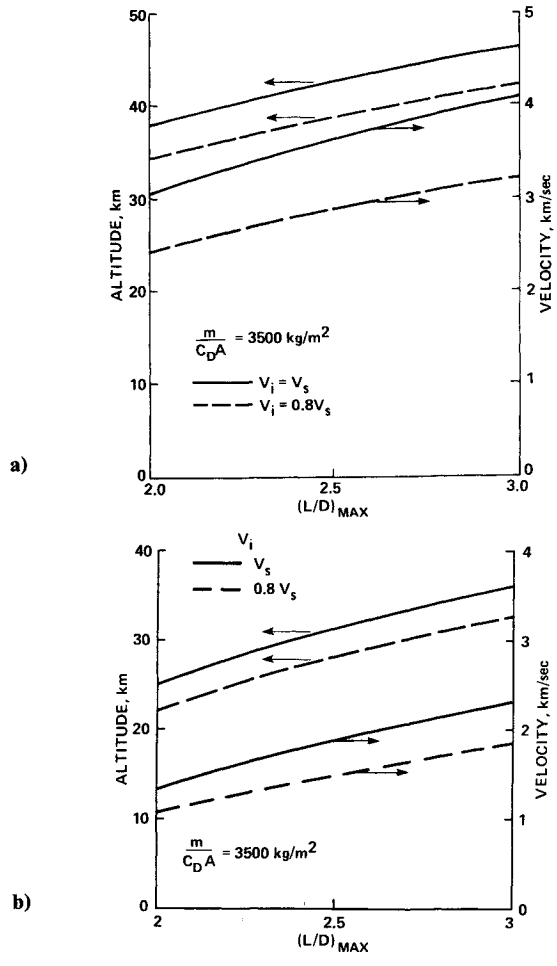

Fig. 5 Flight conditions at end of turns: a) $\Delta\psi = 90$ deg; b) $\Delta\psi = 180$ deg.

For maximum maneuvering capability, high L/D's are required. To achieve a high L/D, a vehicle must have low drag; therefore, the ballistic coefficients at maximum L/D tend to be large. A ballistic coefficient of 3500 kg/m^2 was used for the remainder of the study.

In Figs. 5a and 5b, the ending flight conditions are presented for turns initiated upon entry, at 7.9 km/s and 80% of entry speed (6.32 km/s). For the 90-deg turn begun at entry, the altitudes at the conclusion of the turn vary from 37 km to

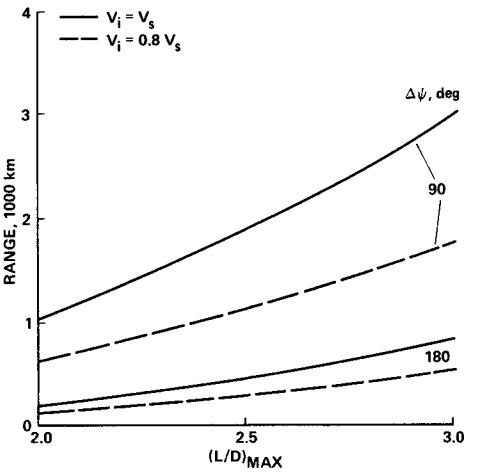

Fig. 6 Residual range after completion of turns.

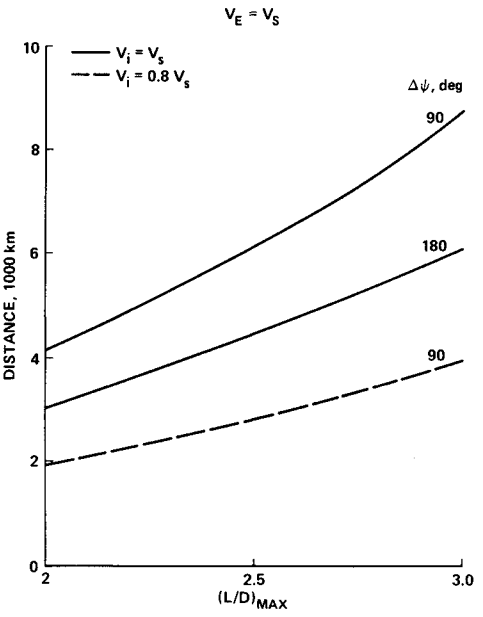

Fig. 7 Lateral ranges for gliding entries.

about 46 km and the velocities from 3.1 to 4.1 km/s. As expected, the final altitudes and velocities for the 180-deg turn are substantially less than for the 90-deg turn. Note that, upon concluding the turns, the vehicle retains substantial kinetic energy and potential energy. Obviously, this remaining energy can be used to glide farther. The residual range [see Eq. (36)] in unbanked flight is shown in Fig. 6. Following a 90-deg turn, the vehicle can glide as much as 1000 km to 3000 km, depending on its maximum L/D. However, the gliding range after a 180-deg turn is much less, varying from less than 200 km to a maximum of 850 km.

The lateral range covered during the turns is shown in Fig. 7. For the 90-deg turn, the distances shown in Fig. 7 determine the landing footprint width. Note that, by beginning the turn at 6.32 km/s, the lateral range is decreased by more than 50%. Also note that, for a 180-deg turn, lateral distances from 3000 to 6000 km can be covered.

The maximum achievable lateral range is shown in Fig. 8 as a function of L/D. The solid line is calculated using Eqs. (34b) and (34c). The dashed line comes from numerically integrating Eq. (33) using the optimum bank angles from Eq. (26) and adding the residual range given by Eq. (36). For $L/D = 2$ to about 2.6, the two methods give nearly the same lateral range. However, at higher L/D's, the present formulation provides a slightly greater lateral range. Both curves have been extended to a lateral distance of 10,000 km, which provides a global

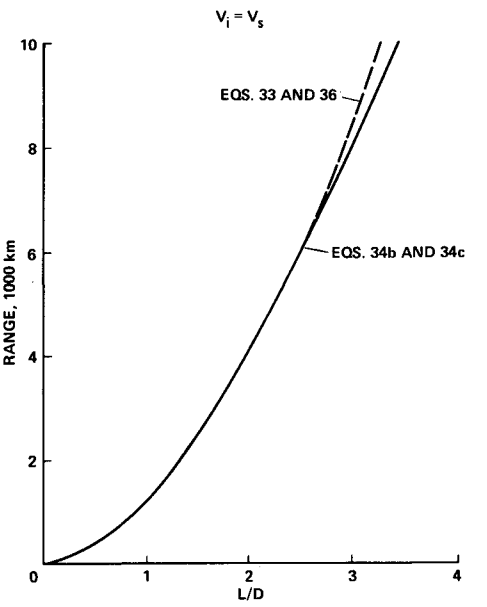

Fig. 8 Maximum lateral range.

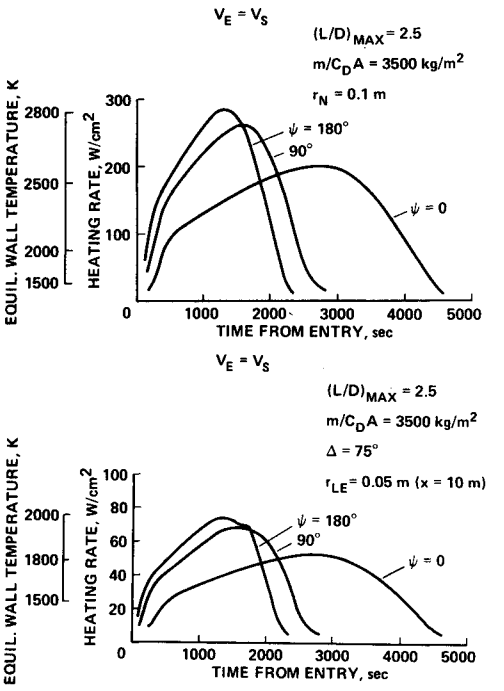

Fig. 9 Entry heating pulses: a) stagnation point; b) wing leading edge.

choice of landing sites. (The vehicle can land at any location within a hemisphere of the entry point. However, since atmospheric entry can be chosen at any point in the orbit, the vehicle can land anywhere on Earth.) The maximum L/D required to achieve global landing coverage is 3.40 using the equations from Ref. 14, whereas the present method[10] predicts a value of 3.23, which is 5% less. Since such high L/D's are very difficult to achieve at hypersonic speeds, the 5% reduction may be important.

Lastly, the heating pulses are compared for the longitudinal glide, the 90-deg turn lateral glide, and the 180-deg-turn case. A peak L/D of 2.5 is assumed and the heating rates are shown as a function of time from entry, for the stagnation point (Fig. 9a) and the wing leading-edge point (Fig. 9b). Because the effective lift/drag ratio ($L/D \cos\phi$) decreases with increasing bank angle, the vehicle flies at a lower altitude at a given speed, thus increasing the heating rates by up to 40% for a 180-deg turn. However, flying at a lower altitude also causes the vehicle

to decelerate faster. Therefore, the heating pulses are substantially shorter in turning flight than in straight flight. In fact, the Shuttle's entry trajectory is modulated by varying the bank angle from +60 to −60 deg at high speeds to reduce the total heat input by nearly 30%, since the total heating is approximately proportional to $(\cos\phi)^{\frac{1}{2}}$.

Concluding Remarks

Although skipping vehicles can attain longer ranges than gliding vehicles, the first flight path has many other disadvantages. Even for entry angles of less than 10 deg, the deceleration loads can be an order of magnitude higher; therefore, the crew of a skipping vehicle experiences severe physiological stresses. To withstand the increased structural loads, such major components as the fuselage and wings must be two to three times heavier, respectively. Also, the heating rates during skipping flight are four to five times higher for an entry angle of only 5.73 deg; skipping flight requires a much more extensive and heavier thermal protection system than does gliding flight.

The study of aerodynamic maneuvers was limited to gliding flight because the environment is much more benign. For the case consisting of a 90-deg turn initiated at entry, the velocity and altitude at the end of the maneuver were 4 km/s and 45 km, respectively, for a vehicle with a maximum L/D of 2.9. Such a high L/D vehicle is able to glide another 2750 km after completing the turn to achieve a total lateral range of 8000 km. The same hypothetical vehicle can make a 180-deg high-speed turn during which a lateral distance of 5000 km would be covered; however, at the end of the turn, the velocity is only 2.2 km/s, which yields an additional range of 750 km. The present lateral-range calculations also showed that a choice of global landing sites can be achieved with $L/D = 3.23$, which is a 5% lower L/D value than had been obtained from previous formulations.

The aerodynamic heating of the vehicle is affected strongly by maneuvering. The peak heating rate increases by approximately 30 and 40% during 90- and 180-deg turns, respectively, compared to unbanked flight. Although the heating rates increase, the total heat input is reduced substantially. During maneuvers, the vehicle loses altitude more rapidly and, thus, decelerates faster than in longitudinal flight, thereby decreasing the duration of the heating pulse.

References

[1]Eggers, A. J., Allen, H. J., and Neice, S. E., "A Comparative Analysis of the Performance of Long-Range Hypervelocity Vehicles," NACA TR-1382, 1958.

[2]Russel, W. R., ed., "Space Shuttle Transportation System—Operational Aerodynamic Data Book," STS85-0118, Sept. 1985.

[3]Marvin, J. G. and Deiwert, G. S., "Convective Heat Transfer in Planetary Gases," NASA TR R-224, July 1965.

[4]Marvin, J. G. and Pope, R. B., "Laminar Convective Heating and Ablation in the Mars Atmosphere," *AIAA Journal*, Vol. 5, Feb. 1967, pp. 241–248.

[5]Arthur, P. D., Shultz, H., and Guard, F. L., "Flat Plate Turbulent Heat Transfer at Hypervelocities," *Journal of Spacecraft and Rockets*, Oct. 1966, pp. 1549–1551.

[6]Tauber, M. E., Menees, G. P., and Adelman, H. G., "Aerothermodynamics of Transatmospheric Vehicles," *Journal of Aircraft*, Sept. 1987, pp. 594–602.

[7]Rubesin, M. W., "The Effect of Boundary Layer Growth Along Swept-Wing Leading Edges," Vidya Corp., Palo Alto, CA, Rept. 4, 1958.

[8]Morkovin, M. V., "Critical Evaluation of Transition from Laminar to Turbulent Shear Layers with Emphasis on Hypersonically Traveling Bodies," Air Force Flight Dynamics Lab., AFFDL-TR-68-149, March 1969.

[9]Throckmorton, D. A., "Benchmark Determination of Shuttle Orbiter Entry Aerodynamic Heat-Transfer Data," *Journal of Spacecraft and Rockets*, Vol. 20, May–June 1983, pp. 219–224.

[10]Tauber, M. E., "Hypervelocity Gliding Maneuvers," *Journal of Aircraft*, Aug. 1987, pp. 572–574.

[11]Slye, R. E., "An Analytical Method for Studying the Lateral Motion of Atmosphere Entry Vehicles," NASA TN D-325, 1960.

[12]Tauber, M. E., "Scaling Relations for Heating During Gliding Entry at Parabolic Speed," *AIAA Journal*, Dec. 1986.

[13]Eggers, A. J., Jr., "The Possibility of a Safe Landing," *Space Technology*, edited by H. S. Seifert, Wiley, New York, 1959, Chap. 13.

[14]Shkadov, L. M., Bukhanova, R. S., Illarionov, V. F., and Plokhikh, V. P., "Mechanics of Optimum Three-Dimensional Motion of Aircraft in the Atmosphere" (1972), NASA TT F-777, March 1975.

[15]Bate, R. R., Mueller, D. D., and White, J. E., *Fundamentals of Astrodynamics*, Dover, New York, 1971.

[16]Corning, G., *Supersonic and Subsonic CTOL and VTOL Airplane Design*, 4th ed., Published by the author, College Park, MD, 1976.